IOP Publishing J. Phys. Mater. 4 (2021) 034005 https://doi.org/10.1088/2515-7639/abf546

Journal of Physics: Materials

OPEN ACCESS

RECEIVED
31 December 2020

REVISED
17 March 2021

ACCEPTED FOR PUBLICATION
6 April 2021

PUBLISHED
21 April 2021

PAPER

Ultrafast electron–hole relaxation dynamics in CdS nanocrystals

Mahima Makkar[1,2], **Luca Moretti**[3], **Margherita Maiuri**[3], **Giulio Cerullo**[3] and **Ranjani Viswanatha**[1,2,4,*]

[1] New Chemistry Unit, Jawaharlal Nehru Centre for Advanced Scientific Research, Jakkur, Bangalore 560064, India
[2] School of Advanced Materials, Jawaharlal Nehru Centre for Advanced Scientific Research, Jakkur, Bangalore 560064, India
[3] IFN-CNR, Dipartimento di Fisica, Politecnico di Milano, Piazza L. da Vinci 32, 20133 Milano, Italy
[4] International Centre for Materials Science, Jawaharlal Nehru Centre for Advanced Scientific Research, Jakkur, Bangalore 560064, India
[*] Author to whom any correspondence should be addressed.

E-mail: rv@jncasr.ac.in

Keywords: pump-probe spectroscopy, II-VI semiconductor nanocrystals, charge carrier dynamics, intraband relaxation

Supplementary material for this article is available online

Abstract

Surface traps significantly influence the charge carrier dynamics within semiconductor nanocrystals, introducing non-radiative exciton recombination channels which are detrimental for their applications. Understanding the nature of these trap states and modulating them synthetically bears immense potential in designing defect-free colloidal semiconductor nanocrystals for efficient optoelectronic devices. Thus, systems devoid of surface traps can be used to study the relaxation pathways of excitons generated within these nanocrystals. In this work, we study the ultrafast charge carrier relaxation dynamics upon near-edge resonance excitation and above-resonance excitation in CdS nanocrystals using ultrafast transient absorption spectroscopy, in order to understand intraband cooling and mid-gap trap states. The time-resolved studies reveal that the above bandgap excitation results in a three-step process, including instantaneous growth followed by a fast sub-picosecond decay and a long-lived (>1 ns) excited state or a trap state recombination. The large percentage of long-lived excitons in CdS nanocrystals elucidates the defect-free nature of the system arising from the absence of surface states.

1. Introduction

Semiconductor nanocrystals (NCs) serve as promising functional materials in solar energy conversion [1], optoelectronics [2], biological imaging [3] etc due to their tunable size and shape-dependent quantum effects. The electronic structure [4, 5] and origin of these size and shape-dependent properties [6] have also been a subject of great interest in fundamental research. Due to the strong three-dimensional quantum confinement when the radius is smaller than the exciton Bohr radius, they present sharp, atom-like transitions between the discrete hole and electron levels, whose energies depend on the NC size. Also, the quantum efficiency of radiative recombination displayed by semiconductor NCs exceeds that of their bulk counterparts, due to the strong overlap between the spatially confined hole and electron wave functions, while excitons within the bulk semiconductors can easily dissociate leading to trapping of charge carriers.

Although the optical properties of NCs are mainly determined by the internal structure of the semiconductor, as the particle size decreases, the contribution of incompletely bonded surface atoms increases [7]. The energy of these surface trap states generally lies within the bandgap, leading to trapping of charge carriers that prevents other useful photoinduced processes, like radiative recombination in photoemissive materials or charge separation in photovoltaic materials. Thus, it is important to suppress the surface trap states in order to increase the device efficiency. Understanding the nature of these trap states and controlling their occurrence, especially with surfaces playing a large role due to the large surface to volume ratio in NCs, has recently gained a lot of attention [8–10].

Further, the device photophysics/chemistry of these NCs is largely determined by the relaxation dynamics of the photoexcited electrons/holes. Thermalization of hot carriers is normally a fast process occurring on

sub-picosecond time scales [11, 12] and is a major factor determining the power conversion efficiencies of optoelectronic devices based on NCs. This intraband relaxation is much faster than the radiative interband recombination (occurring on the nanosecond timescale) and has been the focus of various research directions like intraband lasing [13], mid-infrared light sources and detectors [14] depending on different stages of carrier cooling. For instance, hot carrier relaxation should happen before photon emission in the case of quantum dot lasers [15]. On the other hand, optimization of solar energy conversion efficiency is highly dependent on the utilization of hot carriers before they cool down [16, 17]. Thus it is important to characterize and control intraband carrier relaxation rates that can also be utilized to understand the host-dopant interactions in doped semiconductor NCs.

Understanding trap states essentially boils down to an understanding of the interaction of the host with very specific surface functionalization. The surface capped ligands can modulate the charge carrier relaxation affecting the carrier cooling dynamics [18, 19]. The ligand shell enfolds the semiconductor in a potential well so that the charges are concentrated within the core isolated from the surface, which has minimal impact on photoexcited charge carriers. Additionally, it has been shown that Auger-type recombination is mainly responsible for hot electron cooling [20]. However, surface ligands contribute to the hot hole relaxation via non-adiabatic pathway [21, 22]. Thus it is important to study the carrier cooling dynamics, as it has a direct impact on the performance of these NCs within optoelectronic devices. The femtosecond pump-probe technique is an ideal tool to shed light on carrier population dynamics in these NCs on a timescale of hundreds of femtoseconds to nanoseconds.

In this work we study the intraband relaxation of CdS NCs at near resonance and above-resonance excitations, where these NCs are known to have well-defined intraband transitions. The colloidally synthesized CdS NCs were further overgrown with CdS shells (S-surface coverage being the last shell) to reduce the surface defects. Further, S^{2-} on the surface increases the photooxidative degradation potential reducing the surface defects [23]. The defect states have been suggested to play an important role in excitation dynamics and carrier transport [24–26]. However, our observation of long-lived excitonic states in CdS can be linked to the absence of defect/surface states in these NCs. When exciting above bandgap, we time-resolve a quick, sub-picosecond intraband relaxation to the bandgap exciton, followed by a long-lived photobleaching (PB) signal. These results indicate a negligible weight of competing relaxation channels and demonstrate the high quality of the CdS NCs, with a low density of surface defects.

2. Experimental section

2.1. Materials and synthesis

Cadmium oxide (CdO), oleic acid (OA, 90%), 1-octadecene (ODE, 90%), oleylamine (OlAm, 70%), and sulfur powder (S, 99.5%) were purchased from Sigma Aldrich. All these chemicals were used without further purification.

2.2. Precursors for synthesis

Cadmium oleate, a precursor for the synthesis of CdS NCs, was synthesized using CdO. OA and octadecene were used as coordinating solvents. For the synthesis of 0.2 M cadmium oleate, 0.3204 g CdO, 9 ml of ODE and 7 ml of OA were taken in a three-necked round bottom flask. The system was degassed at 80 °C for two hours under constant stirring. The temperature was raised to 250 °C after degassing and kept under argon flow. The system was kept for about 2 min until the precursors were completely dissolved and a clear solution was obtained. It was then cooled down to room temperature. S-ODE, S-precursor for the synthesis of CdS nanostructures, was synthesized using sulfur powder. For the synthesis of 0.2 M S-ODE, 65 mg of sulfur powder and 10 ml of ODE were taken in a vial. The system was degassed at room temperature for 15–20 min. Argon was purged. Sonication and heating were performed to obtain a clear solution.

2.3. Synthesis of CdS NCs

CdS core was synthesized and was further overcoated with CdS multilayers. Cadmium oleate of 0.2 M (0.5 ml) and ODE (4 ml) were taken in a three-necked flask and degassed at 80 °C. After 2 h of degassing, the temperature was raised to 280 °C under constant Ar atmosphere and 0.2 M S-ODE (0.8 ml) was quickly injected into the reaction mixture, with sulfur precursor being in excess to avoid S^{2-} vacancies, thus reducing the surface defects. The temperature was quickly brought down to 250 °C and 3 ml of OlAm was added to the reaction mixture. Further, CdS shells were grown using the successive ionic layer adsorption and reaction (SILAR) technique [27]. As S^{2-} vacancies are major contributors to surface defects [7], we have made sure that the system is rich in sulfur at every synthesis step. The core CdS nanoparticles were synthesized with excess sulfur. Further, the overcoating was initiated with sulfur precursor addition and the last step of the

overcoating was also the addition of the sulfur precursor, where S^{2-} on the surface makes the system less susceptible to photooxidative degradation.

2.4. Characterization

Transmission electron microscopy (TEM) was performed on a Tecnai F30 UHR version electron microscope, using a field emission gun operating at an accelerating voltage of 200 kV in bright field mode using Cu coated holey carbon TEM grids. Powder x-ray diffraction (XRD) pattern for the NCs was recorded on a Bruker D8 advance diffractometer using Cu–K_α radiation (1.5418 Å). For recording the absorption spectra, the samples were dissolved in hexane and loaded in quartz cuvettes. A blank cuvette containing only hexane was used as a reference. The optical absorption spectra were obtained using an Agilent 8453 UV visible spectrometer. Pump-probe measurements were carried out using an amplified Ti:sapphire laser (Coherent Libra) as source, with maximum output energy of about 4 mJ, 1 kHz repetition rate, a central wavelength of 800 nm and pulse duration of about 100 fs. A fraction of the laser output was split to generate the required pulses. One part was used for generating the excitation (pump) pulses: the pump at 400 nm (3.1 eV) was generated by frequency doubling in a β-barium borate crystal, while the pump at 480 nm (2.58 eV) was generated using optical parametric amplification in a β-barium borate crystal. Pump pulses were modulated by a mechanical chopper at a 500 Hz repetition rate and were delayed in time using a mechanical stage. Finally, the pump was focused with a lens to obtain a fluence of around 24 μJ cm^{-2}. The other part of the beam was used to generate the probe pulses by the white light continuum generation process, by focusing the 800 nm beam into a thin calcium fluoride plate, obtaining a spectrum ranging from 340 nm (3.65 eV) to 700 nm (1.77 eV). The probe pulse was focused on the sample non-collinearly with the pump beam and the spectrum of the transmitted probe beam was measured by an optical multichannel analyzer (OMA) working at the full 1 kHz laser repetition rate. Thanks to the modulation of the pump pulse, two consecutive probe pulses measure the sample in the excited and the ground state. By measuring their corresponding intensities (I_{on} and I_{off}) one can calculate the normalized transmission change: $\Delta T/T = (I_{on}/I_{off}) - 1$, both as a function of wavelength (OMA detection) and time delay (mechanical delay). Chirp-free transient absorption spectra were obtained by using a dechirping algorithm.

3. Results and discussion

CdS NCs were obtained via colloidal synthesis and further overcoated with shells of CdS using the SILAR [27] technique to minimize the density of surface trap states. The careful control over the synthesis allowed precise engineering of defects. Further, thicker shells achieved through SILAR overcoating can quarantine a core exciton state and reduce the interaction between a core exciton state and the surface traps, leading to long-lived excitonic bleaching [28, 29]. The XRD pattern, as shown in figure S1 (available online at stacks.iop.org/JPMATER/4/034005/mmedia), confirms the presence of hexagonal (space group) CdS NCs without any impurities. The reference XRD pattern for CdS (obtained from the inorganic crystal structure database) is also shown in figure S1. The particles exhibit uniform spherical morphology with a diameter of 12 $\pm$ 0.7 nm, as shown by the TEM image in figure S2. Figure 1 shows the absorption spectrum, with an onset at around 2.45 eV, along with a typical differential transmission ($\Delta T/T$) spectrum at 0.5 ps, following photoexcitation at 3.1 eV. The decay dynamics of CdS NCs were studied using a femtosecond transient absorption technique with a pump fluence of 24 μJ cm^{-2} and acquired at 3.1 eV and 2.58 eV photoexcitation energies. The 3.1 eV (400 nm) pump photon energy corresponds to an off-resonance excitation above the bandgap for CdS NCs ($\sim$2.54 eV), while the 2.58 eV (480 nm) excitation is in near resonance with the first excitonic transition of CdS NCs, as shown by dotted lines in figure 1.

Figure 2(a) shows the time trace of the $\Delta T/T$ signal at probe energy of 2.54 eV upon excitation with pump energy of 3.1 eV. We observe a positive signal due to ground state bleaching (GSB) of the excitonic transition. The trace displays a relatively fast rise, followed by fast decay for the first 20 ps with almost no further decay within the time frame of the study. The initial fast decay within the first few ps cannot be a result of electron–hole recombination. Hence it could either be the intraband cooling or the non-radiative recombination into the trap states. The schematic shown in figure 2(b) shows the probable paths with the quantum mechanical states of the CdS NCs [30] as well as the trap states and/or Auger recombination states as observed from the data in figure 2(a). However, upon zooming into the rise, we observe that this rise is not instantaneous within the instrumental response function (IRF) of the pump-probe apparatus, but rather takes a finite time, as shown in the inset to figure 2(a). To study the path of excited carriers, we have fitted the curve with a single exponential build-up followed by a biexponential decay as shown by the solid line in figure 2(a). From this fit, we obtain the time constant of growth to be 460 $\pm$ 10 fs and the decay time constants to be 4.85 $\pm$ 0.2 ps and >1000 ps. The data indicate that about 90% of the signal does not decay within the timeframe of our observation, suggesting the high quality of the sample with very small

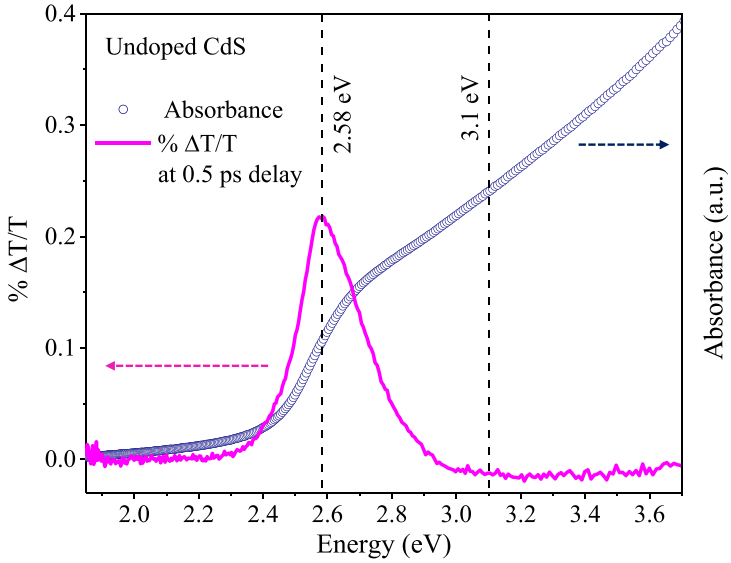

Figure 1. Absorption and differential transmission spectrum (at 0.5 ps delay) for CdS NCs. The dotted lines show the near-resonance and off-resonance pump photon energy.

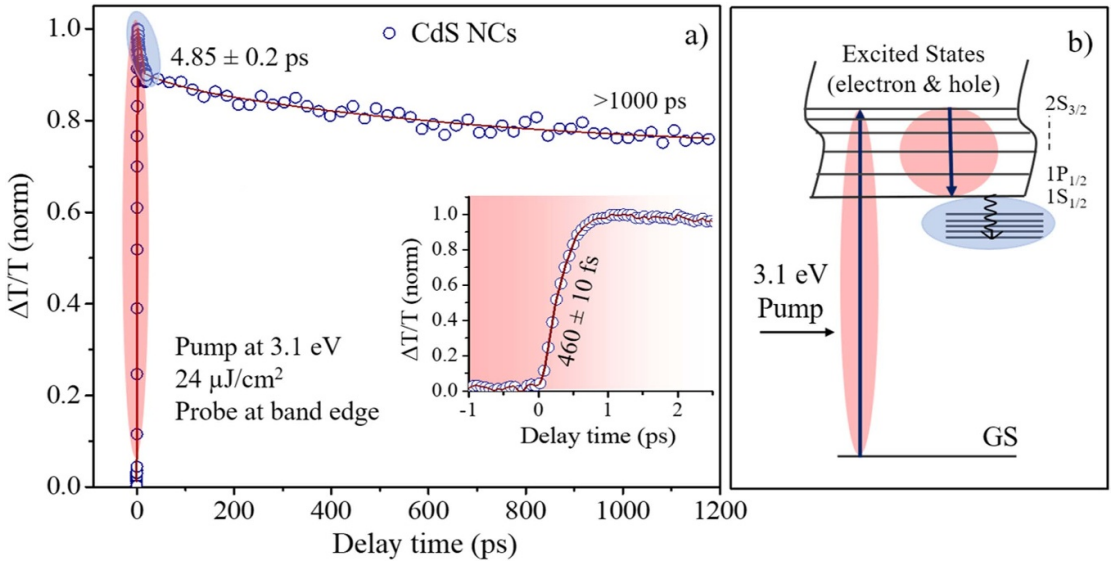

Figure 2. (a) Differential transmission dynamics for CdS NCs under 3.1 eV (400 nm) laser excitation with a fluence of 24 μJ/cm^{-2}. Inset: zoom-in of the dynamics up to 2.5 ps. (b) Schematic representing the process of non-resonant excitation, intraband relaxation and decay into trap states for CdS NCs.

non-radiative recombination sites like the surface trap states. The decay constant of 4.85 ± 0.2 ps can be assigned either to the Auger processes or to the recombination via surface trap states. However, its intensity is observed to be 10% or smaller at the band gap energy. Most interestingly, the finite build-up time of the $\Delta T/T$ signal at the band edge energy suggests the gradual population of the charge carriers at the band edge. Following the instantaneous excitation of higher excited states (ES) of CdS, we assign the growth time to the relaxation of the charge carriers respectively to the conduction band minimum (CBM) and valence band maximum in a finite time frame, thus slowly populating the 1S–1S$_{1/2}$ transition at 2.49 ± 0.01 eV. If this is indeed true, the growth and decay should change as a function of probe energy. The observation that the decay of the GSB signal of the higher energy states is complete within the growth time of the GSB of the band edge state would imply that the relaxation of both hot electrons and hot holes occurs within this time interval, with no intervention from either electron or hole traps. On the other hand, the observation that the GSB recovery is incomplete at higher energies would imply that there exist two ES that share the same ground state and hence demonstrate the presence of electron/hole trap states that can compete with the intraband cooling.

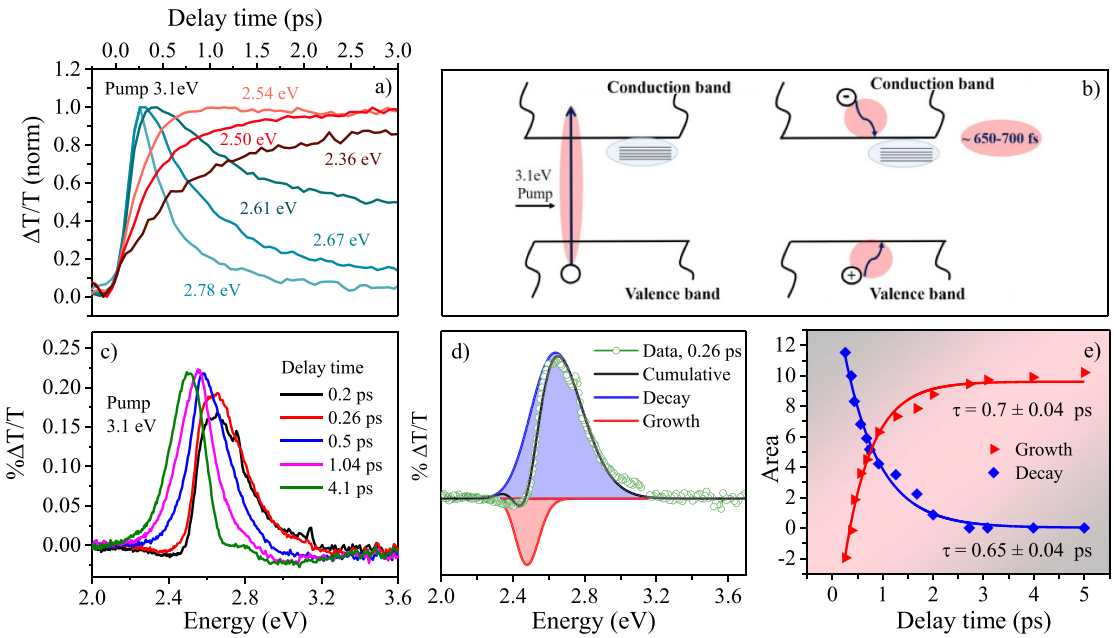

Figure 3. (a) Differential transmission dynamics for CdS NCs up to 3 ps at different probe energies under non-resonant excitation (3.1 eV). (b) Schematic describing the excitation and intraband cooling process under non-resonant excitation (c) differential transmission spectra of CdS NCs measured at different pump-probe delays at 400 nm (3.1 eV) excitation. (d) Typical fitting of the $\Delta T/T$ spectrum obtained at a delay of 0.26 ps with two Gaussian peaks corresponding to excitonic states at 2.49 ± 0.01 eV and 2.63 ± 0.01 eV. (e) The area under these peaks at various delay times are plotted as red and blue diamonds while the solid line is a fit to a single exponential decay/growth with the given time constants.

To clarify the cooling dynamics in CdS NCs, we studied differential transmission decays as a function of the probe energy at 3.1 eV excitation. Figure 3(a) shows the time plots at various probe photon energies. Interestingly, high probe energies highlight not only an instantaneous rise of the GSB signal but also a rapid and complete decay, suggesting a simultaneous decay of both the hot charge carriers. On the other hand, at lower probe energies there is a clear build-up time, on the picosecond timescale, followed by saturation suggesting that the CBM is being populated due to the relaxation from higher ESs, as shown in the schematic in figure 3(b).

Figure 3(c) reports a sequence of $\Delta T/T$ spectra at different delays. We performed a global analysis using the least square error minimization method on these spectra by fitting them to the sum of two Gaussians, with the energy of one of the Gaussians being fixed to 2.49 ± 0.01 eV, which corresponds to the lowest $1S–1S_{1/2}$ excitonic state. The energy of the higher ES corresponds to 2.63 ± 0.01 eV, with a gap of 140 meV between the two states. Based on the theoretical calculations of energy levels of CdS NC reported in the literature [30], we assign this ES to the $1S–2S_{3/2}$ transition. A sample fit at early times is shown in figure 3(d). The 2.63 ± 0.01 eV peak decays to zero within a few picoseconds, implying a complete relaxation of both the hot charge carriers while the 2.49 ± 0.01 eV peak grows in and does not appreciably decay on the picosecond timescale.

The area under the curve for the two Gaussians (red and blue symbols) is plotted as a function of probe delay time and the corresponding fits to these two dynamics at 2.49 eV ± 0.01 and 2.63 ± 0.01 eV are shown as solid lines in figure 3(e). The time constants obtained after fitting with a single exponential decay/growth are observed to be similar for both the signals, that is, 700 ± 40 fs for the growth of the band edge peak and 650 ± 40 fs for the decay of higher ES, suggesting that one state is growing at the expense of the other. Thus, the observed time-dependent red-shift of the $\Delta T/T$ spectrum in the first few picoseconds is understood in terms of intraband relaxation.

To confirm that this fast decay is indeed from intraband relaxation and not any other non-radiative pathways, we excited the system near resonance (excitation at 2.58 eV) and investigated the decay dynamics and energy dependence of the differential transmission spectra, as shown in figure 4. At near-resonant excitation, we observe a transient GSB with an IRF-limited fast rise (<100 fs) followed by an additional sub-picosecond evolution and a long-lived excited state, as shown in the $\Delta T/T$ dynamics for different probe energies in figure 4(a) and at the band-edge up to 1200 ps in figure S3, SI.

The differential transmission dynamics are nearly independent of the probe energy as the excitation is carried out at near resonance and hence with little excess energy. This excitation condition is further reflected

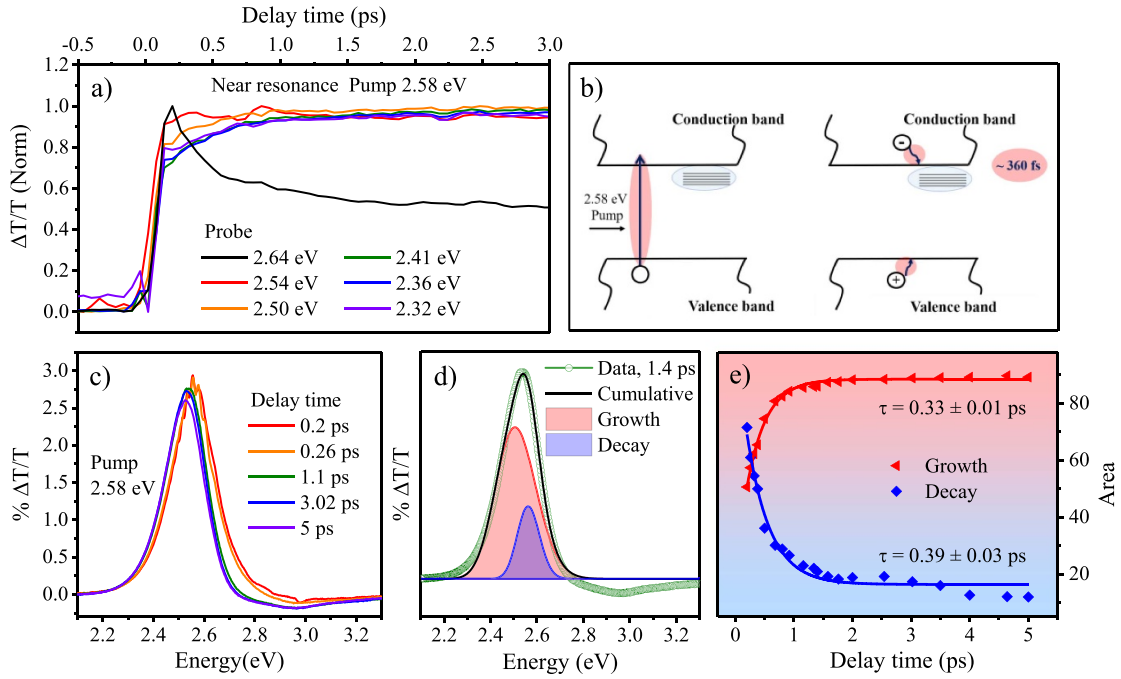

Figure 4. (a) Differential transmission dynamics for CdS NCs up to 3 ps at different probe energies under near-resonance excitation (2.58 eV). (b) Schematic describing near-resonance excitation and intraband cooling. (c) Differential transmission spectra of CdS NCs measured at different pump-probe delays at 2.58 eV (480 nm) excitation. (d) Typical fitting of the $\Delta T/T$ spectrum obtained at a delay of 1.4 ps with two Gaussian peaks at $2.56 \pm 6.8 \times 10^{-4}$ eV and $2.50 \pm 4.5 \times 10^{-4}$ eV. (e) The area under these deconvoluted peaks at various delay times plotted as red triangles ($2.50 \pm 4.5 \times 10^{-4}$ eV) and blue diamonds ($2.56 \pm 6.8 \times 10^{-4}$ eV) while the solid line is a single exponential decay/growth fit with the given time constants.

in the schematic in figure 4(b). Additionally, the $\Delta T/T$ spectrum for the 2.58 eV laser excitation can be largely characterized by a GSB peak centered around $2.50 \pm 4.5 \times 10^{-4}$ eV, characteristic of the bandgap exciton spectrum as shown in figure 4(c). Deconvolution of these spectra using global analysis demonstrates the presence of two states, one at an energy of $2.56 \pm 6.8 \times 10^{-4}$ eV, while the second at the band edge or $1S\text{-}1S_{1/2}$ state at $2.50 \pm 4.5 \times 10^{-4}$ eV and a sample fit at early times is shown in figure 4(d). The $2.50 \pm 4.5 \times 10^{-4}$ eV state arises from the same states in the two experiments at near-resonance ($2.50 \pm 4.5 \times 10^{-4}$) and above-resonance excitation (2.49 ± 0.01 eV) cases and are the same within the experimental error. We believe that the $2.56 \pm 6.8 \times 10^{-4}$ eV peak arises from the vibrationally excited state and not an electronically excited state. This is concluded based on the quick time scale of its decay as well as the narrow full width half maximum (FWHM) of the peak. It is quite possible that this component exists even in the off-resonance case along with several other components. However, it is impossible to de-convolute all the components with a high degree of confidence, and hence we have only deconvoluted the major components arising from the electronic states of the NCs. Kinetic traces demonstrate that the decay of the higher ES has a time constant (390 ± 30 fs) that is very similar to the time constant (330 ± 10 fs) obtained for the growth of CBM as shown in figure 4(e). This confirms the nature of intraband relaxation that the carriers undergo after excitation. As compared to the non-resonant case wherein higher electronic states could be accessed, intraband cooling in the near-resonant excitation is much faster as expected [31]. Taken together, our experimental data show that the fast dynamics observed on the sub-picosecond timescale are due to intraband relaxation. Further, it is important to note that these samples are largely free of surface trap states as evidenced by the long-lived PB component that is essentially constant over the ≈1 ns observation time window, suggesting them to be good candidates for any photovoltaic or photoemissive device application.

4. Conclusion

Our pump-probe studies on high-quality CdS NCs prepared via colloidal SILAR technique show that the band edge states are populated by the simultaneous decay of hot electrons and holes over a period of several hundreds of femtoseconds. The low density of surface states in the NC allows for a long-lived excited state as accessed by pump-probe measurements and is suitable for radiative recombination. We also develop an understanding of the processes involved in charge carrier dynamics starting from the excitation to the carrier

stabilization where the multi-component behavior is associated with the growth, intraband cooling and a long-lived excited state component that does not decay up to 1000 ps. Decoupling of growth and intraband relaxation could be achieved only with the above band-gap excitation unlike the resonant case and it can further be employed for applications. Our attempt to study these hot carriers and what happens to them before cooling to thermal equilibrium was possible in our case because of the long-lived excitonic bleaching of the excited state. The relatively long carrier lifetimes with small recombination coefficient and the slow thermalization dynamics of hot carriers are believed to originate from the protection offered to these carriers in the absence of surface trap states. Thus, this robust system can be utilized to study the intraband transitions and associated processes that occur on similar time scales like dopant–host interactions within the doped semiconductors.

Data availability statement

All data that support the findings of this study are included within the article (and any supplementary files).

Acknowledgments

The authors thank JNCASR, Sheikh Saqr Laboratory, Science and Engineering Research Board, Department of Science and Technology, Government of India, for financial support.

Conflict of interest

The authors declare no competing interests.

ORCID iDs

Mahima Makkar https://orcid.org/0000-0002-2804-9733
Luca Moretti https://orcid.org/0000-0001-8092-0752
Ranjani Viswanatha https://orcid.org/0000-0002-3819-4029

References

[1] Klimov V I 2006 Mechanisms for photogeneration and recombination of multiexcitons in semiconductor nanocrystals: implications for lasing and solar energy conversion (ACS Publications)
[2] Isshiki M and Wang J II-IV 2017 Semiconductors for optoelectronics: CdS, CdSe, CdTe *Springer Handbook of Electronic and Photonic Materials* (Berlin: Springer) pp 1–1
[3] Kairdolf B A, Smith A M, Stokes T H, Wang M D, Young A N and Nie S 2013 Semiconductor quantum dots for bioimaging and biodiagnostic applications *Annu. Rev. Anal. Chem.* **6** 143–62
[4] Grandhi G K, Tomar R and Viswanatha R 2012 Study of surface and bulk electronic structure of II–VI semiconductor nanocrystals using Cu as a nanosensor *ACS Nano* **6** 9751–63
[5] Grandhi G K, Swathi K, Narayan K S and Viswanatha R 2014 Cu doping in ligand free CdS nanocrystals: conductivity and electronic structure study *J. Phys. Chem. Lett.* **5** 2382–9
[6] Ngo C Y, Yoon S F, Fan W J and Chua S J 2006 Effects of size and shape on electronic states of quantum dots *Phys. Rev.* B **74** 245331
[7] Veamatahau A, Jiang B, Seifert T, Makuta S, Latham K, Kanehara M, Teranishi T and Tachibana Y 2015 Origin of surface trap states in CdS quantum dots: relationship between size dependent photoluminescence and sulfur vacancy trap states *Phys. Chem. Chem. Phys.* **17** 2850–8
[8] Grandhi G K and Viswanatha R 2016 Understanding the role of surface capping ligands in passivating the quantum dots using copper dopants as internal sensor *J. Phys. Chem.* C **120** 19785–95
[9] Flatae A M, Tantussi F, Messina G C, De Angelis F and Agio M 2019 Plasmon-assisted suppression of surface trap states and enhanced band-edge emission in a bare CdTe quantum dot *J. Phys. Chem. Lett.* **10** 2874–8
[10] Giansante C and Infante I 2017 Surface traps in colloidal quantum dots: a combined experimental and theoretical perspective *J. Phys. Chem. Lett.* **8** 5209–15
[11] Klimov V I 2000 Optical nonlinearities and ultrafast carrier dynamics in semiconductor nanocrystals (ACS Publications)
[12] Wehrenberg B L, Wang C and Guyot-Sionnest P 2002 Interband and intraband optical studies of PbSe colloidal quantum dots *J. Phys. Chem.* B **106** 10634–40
[13] Markus A, Chen J X, Gauthier-Lafaye O, Provost J G, Paranthoën C and Fiore A 2003 Impact of intraband relaxation on the performance of a quantum dot laser *IEEE J. Sel. Top. Quantum Electron.* **9** 1308–14
[14] Livache C *et al* 2019 A colloidal quantum dot infrared photodetector and its use for intraband detection *Nat. Commun.* **10** 1–10
[15] Htoon H, Hollingworth J A, Malko A V, Dickerson R and Klimov V I 2003 Light amplification in semiconductor nanocrystals: quantum rods versus quantum dots *Appl. Phys. Lett.* **82** 4776–8
[16] Nozik A J 2002 Quantum dot solar cells *Physica* E **14** 115–20
[17] Nozik A J 2001 Spectroscopy and hot electron relaxation dynamics in semiconductor quantum wells and quantum dots *Annu. Rev. Phys. Chem.* **52** 193–231
[18] Guyot-Sionnest P, Wehrenberg B and Yu D 2005 Intraband relaxation in CdSe nanocrystals and the strong influence of the surface ligands *J. Chem. Phys.* **123** 074709

[19] Peterson M D, Cass L C, Harris R D, Edme K, Sung K and Weiss E A 2014 The role of ligands in determining the exciton relaxation dynamics in semiconductor quantum dots *Annu. Rev. Phys. Chem.* **65** 317–39
[20] Rabouw F T, Vaxenburg R, Bakulin A A, Van Dijk-moes R J A, Bakker H J, Rodina A, Lifshitz E, Efros A L, Koenderink A F and Vanmaekelbergh D 2015 Dynamics of intraband and interband auger processes in colloidal core–shell quantum dots *ACS Nano* **9** 10366–76
[21] Cooney R R, Sewall S L, Dias E A, Sagar D M, Anderson K E H and Kambhampati P 2007 Unified picture of electron and hole relaxation pathways in semiconductor quantum dots *Phys. Rev.* B **75** 245311
[22] Kambhampati P 2011 Unraveling the structure and dynamics of excitons in semiconductor quantum dots *Acc. Chem. Res.* **44** 1–13
[23] Smith A M and Nie S 2010 Semiconductor nanocrystals: structure, properties, and band gap engineering *Acc. Chem. Res.* **43** 190–200
[24] Li W, Long R, Tang J and Prezhdo O V 2019 Influence of defects on excited-state dynamics in lead halide perovskites: time-domain *ab initio* studies *J. Phys. Chem. Lett.* **10** 3788–804
[25] Hoch L B, Szymanski P, Ghuman K K, He L, Liao K, Qiao Q, Reyes L M, Zhu Y, El-Sayed M A and Singh C V 2016 Carrier dynamics and the role of surface defects: designing a photocatalyst for gas-phase CO_2 reduction *Proc. Natl Acad. Sci.* **113** E8011–E8020
[26] Ding J, Lian Z, Li Y, Wang S and Yan Q 2018 The role of surface defects in photoluminescence and decay dynamics of high-quality perovskite $MAPbI_3$ single crystals *J. Phys. Chem. Lett.* **9** 4221–6
[27] Li J J, Wang Y A, Guo W, Keay J C, Mishima T D, Johnson M B and Peng X 2003 Large-scale synthesis of nearly monodisperse CdSe/CdS core/shell nanocrystals using air-stable reagents via successive ion layer adsorption and reaction *J. Am. Chem. Soc.* **125** 12567–75
[28] Sun J, Zhao J and Masumoto Y 2013 Shell-thickness-dependent photoinduced electron transfer from $CuInS_2$/ZnS quantum dots to TiO_2 films *Appl. Phys. Lett.* **102** 053119
[29] Neo D C, Cheng C, Stranks S D, Fairclough S M, Kim J S, Kirkland A I, Smith J M, Snaith H J, Assender H E and Watt A A 2014 Influence of shell thickness and surface passivation on PbS/CdS core/shell colloidal quantum dot solar cells *Chem. Mater.* **26** 4004–13
[30] Horodyská P, Němec P, Sprinzl D, Malý P, Gladilin V N and Devreese J T 2010 Exciton spin dynamics in spherical CdS quantum dots *Phys. Rev.* B **81** 045301
[31] Stoll T, Branchi F, Rehault J, Scotognella F, Tassone F, Kriegel I and Cerullo G 2017 Two-dimensional electronic spectroscopy unravels sub-100 fs Electron and hole relaxation dynamics in Cd-chalcogenide nanostructures *J. Phys. Chem. Lett.* **8** 2285–90